A Quantitative Raman Spectroscopic Signal for Metal−Phosphodiester Interactions in Solution[†]

Eric L. Christian,*,[‡,§] Vernon E. Anderson,[§,||] Paul R. Carey,[§] and Michael E. Harris*,[‡,§]

[‡]*Center for RNA Molecular Biology and* [§]*Department of Biochemistry, Case Western Reserve University School of Medicine, Cleveland, Ohio 44106.* [||]*Current address: National Institute of General Medical Sciences, Building 45-Natcher Building, 2AS43J, 45 Center Dr., Bethesda, MD 20892.*

ABSTRACT: Accurate identification and quantification of metal ion−phosphodiester interactions are essential for understanding the role of metal ions as determinants of three-dimensional folding of large RNAs and as cofactors in the active sites of both RNA and protein phosphodiesterases. Accomplishing this goal is difficult due to the dynamic and complex mixture of direct and indirect interactions formed with nucleic acids and other phosphodiesters in solution. To address this issue, Raman spectroscopy has been used to measure changes in bond vibrational energies due to metal interactions. However, the contributions of inner-sphere, H-bonding, and electrostatic interactions to the Raman spectrum of phosphoryl oxygens have not been analyzed quantitatively. Here, we report that all three forms of metal ion interaction result in attenuation of the Raman signal for the symmetric vibration of the nonbridging phosphate oxygens ($\nu_s PO_2^-$), while only inner-sphere coordination gives rise to an apparent shift of $\nu_s PO_2^-$ to higher wavenumbers ($\nu_s PO_2^- M$) in solution. Formation of $\nu_s PO_2^- M$ is shown to be both dependent on metal ion identity and an accurate measure of site-specific metal ion binding. In addition, the spectroscopic parameter reflecting the energetic difference between $\nu_s PO_2^-$ and $\nu_s PO_2^- M$ ($\Delta\nu M$) is largely insensitive to changes in phosphodiester structure but strongly dependent on the absolute electronegativity and hardness of the interacting metal ion. Together, these studies provide strong experimental support for the use of $\nu_s PO_2^- M$ and $\Delta\nu M$ as general spectroscopic features for the quantitative analysis of metal binding affinity and the identification of metal ions associated with phosphodiesters in solution.

Metal−phosphodiester interactions play central roles as determinants of the three-dimensional structure of nucleic acids and as cofactors in the active sites of both RNA and protein phospho-diesterases (*1−4*). These interactions include electrostatic charge−charge interactions between the positively charged metal and the negatively charged phosphodiester backbone, hydrogen bonding (H-bonding) via coordinated water molecules, and inner-sphere coordination of one or more nonbridging oxygens. These chemical interactions give rise to two general classes of metal ion binding: binding in a stable chelated mode with geometric specificity that often involves inner-sphere coordination and binding in a diffuse mode in which numerous ions interact weakly, primarily via electrostatic interactions with the negatively charged phosphodiester backbone (*5−9*). The extent to which chelated and diffuse metal ion binding occurs is determined by local nucleic acid structure and is likely to include a combination of the three distinct chemical forms of metal−phosphodiester interaction. Quantitative assessment of the distribution of inner-sphere coordination, H-bonding, and electrostatic interactions, however, is still difficult to conduct experimentally. A significant part of this difficulty is due to the dynamic nature of metal−phosphodiester interactions, particularly in

solution, which continues to provide a barrier to a complete understanding of the linkage between ion binding and function. In addition to these challenges, functional RNAs often require the binding of multiple ion species (e.g., Mg^{2+} and Na^+) with distinct and overlapping levels of inner-sphere coordination, H-bonding, and electrostatic effects, making the analysis of individual ion interactions difficult to deconvolute.

An emerging strategy for the direct probing of specific chemical interactions between metal ions and phosphodiesters is based on the principle that these interactions will necessarily perturb the vibrational properties of the interacting atoms of the phosphodiester (*10−12*). Changes in the vibrational properties of bonded atoms have long been monitored by Raman spectroscopy, which measures the exchange of energy between photons and vibrating bonded atoms in a sample (*11*). Thus, when the vibrational properties of individual or groups of energetically coupled bonds are altered (e.g., through the binding of a metal ion), such changes are reported directly as a change in the energy of scattered photons. Indeed, changes in bond vibrations due to the presence of metal ions are readily observed in the Raman spectrum of phosphodiesters, including nucleotides and nucleic acids, and have been used as a semiquantitative method for monitoring metal ion binding (*12−15*). Furthermore, because the time frame of photon scattering is fast relative to molecular motion, the Raman signal is largely immune to the distortions of the experimental signal caused by changes in the molecular structure or type of metal ion interaction while the experimental

*To whom correspondence should be addressed. E.L.C.: e-mail, eric.christian@case.edu; phone, (216) 368-1877. M.E.H.: e-mail, michael.e.harris@case.edu; phone, (216) 368-4779; fax, (216) 368-2010.

signal is being generated (*11*). Thus, under equilibrium conditions, Raman spectroscopy enables the assessment of the distribution of individual atomic interactions in a population of molecules.

One of the largest metal-dependent changes in the Raman spectra of phosphodiesters occurs in the group frequency associated with the symmetric stretch of the nonbridging phosphate oxygens ($\nu_s PO_2^-$) (*13–15*). Experimentally, the Raman peak for $\nu_s PO_2^-$ becomes attenuated and undergoes a large apparent shift to higher wavenumbers in the presence of numerous metal ions common to biological systems (*13–15*). The apparent shift in the position of the $\nu_s PO_2^-$ peak produces an inflection in Raman difference spectra where metal-dependent changes in the Raman spectrum are typically analyzed. The apparent shift of $\nu_s PO_2^-$ to higher wavenumbers has been proposed to reflect an altered vibrational mode involving the nonbridging oxygens (here termed $\nu_s PO_2^- M$) that is induced upon metal ion binding (*14, 16*). Consistent with this interpretation, formation of $\nu_s PO_2^- M$ has been observed to correlate with the loss of fully hydrated magnesium ion and the formation of magnesium penta- or tetrahydrate in crystals of the HDV ribozyme (*12*). Furthermore, quantification of difference spectra has been used to approximate the same number of stable site-bound metal ions in HDV crystals as previously determined by other biochemical and biophysical methods (*12, 17–19*).

Application of Raman spectroscopy to analyzing phosphodiester–metal ion interactions, however, still faces several important challenges. Electrostatic interactions, for example, are known to make thermodynamically large and topologically complex contributions to ion affinity. Thus, while crystallography provides a significantly enhanced spectroscopic signal relative to that in solution, the closely packed geometry of the phosphodiester backbone in crystal lattices and the solvent conditions required for Raman crystallography may result in binding geometries and thermodynamics that may not quantitatively reflect ion binding in solution. In addition, the interpretation of metal-induced changes in $\nu_s PO_2^-$ is complicated by ambiguities in the extent to which inner-sphere coordination, outer sphere H-bonding, and electrostatic interactions contribute to changes in phosphodiester vibrational modes. Resolving this ambiguity and extending the method to quantitative analysis of metal–phosphate interactions in solution are thus essential to the development of this otherwise powerful spectroscopic approach.

To accomplish these goals, we examined ion-induced changes in the nonbridging oxygen vibrational modes in dimethyl phosphate (DMP), nucleotides, and nucleic acids in solution. In addition, we compared the effects of ions that differ in their ability to interact with nonbridging phosphate oxygens by inner-sphere coordination, H-bonding, or electrostatic interactions. These and other studies reveal that all three forms of metal interaction can significantly attenuate the magnitude of $\nu_s PO_2^-$, while the metal-induced vibrational mode ($\nu_s PO_2^- M$) is attributed to purely inner-sphere coordination. Quantitative analysis of the intensity of $\nu_s PO_2^- M$ formation as a function of metal ion concentration is further shown to accurately monitor saturable binding of Mg^{2+} to ATP and ADP. In addition, the degree of the shift of $\nu_s PO_2^-$ to higher wavenumbers by Mg^{2+} and other metal ions is shown to correlate strongly with the absolute electronegativity and absolute hardness of the interacting metal ion, providing a potential means of establishing the identity of interacting metal ions. The spectral characteristics of inner-sphere, H-bonding, and electrostatic metal ion binding described

above are observed for both simple and structurally complex phosphodiesters over a broad range of ionic strength and metal ion type and thus are likely to reflect the behavior of phosphodiesters in general.

METHODS

Reagents. ATP, ADP, $MnCl_2$, and cobalt hexamine were obtained from Sigma. $CaCl_2$, $CoCl_2$, and $ZnCl_2$ were purchased from Fisher Scientific. $CdCl_2$ was obtained from Acros Organics. $MgCl_2$ was purchased from Ambion Inc. DMP and DMTP were synthesized by hydrolysis of dimethyl chlorophosphate and dimethyl chlorothiophosphate (Aldrich). Specifically, individual chlorophosphates were incubated overnight in a 40-fold molar excess of water and dehydrated to near dryness under vacuum. The resulting phophodiesters were then brought to a stock concentration of 0.4 M with water, and the solution was adjusted to pH 5.0 with formate. Eleven-nucleotide single-stranded RNA 5'-UCAAGUACCGA-3', the 12-nucleotide GAAA tetraloop (5'-GGGCGAAAGUCC-3'), and the 27-nucleotide bulged stem–loop sequence derived from the P4 helix/stem–loop portion of RNase P RNA (*20*) (5'-GGAAGUCCGGUCUUCG-GACCGGCUUCC-3') were made by solid phase synthesis (Dharmacon Inc.). Yeast tRNA^PHE and *Escherichia coli* RNase P RNA were prepared by in vitro transcription using standard methods (Ambion). All RNAs were purified on 8–22.5% 19:1 acrylamide/bisacrylamide gels. RNA bands were identified by UV shadowing, cut out of the gel, and eluted overnight at room temperature in 10 gel volumes of 10 mM Tris-HCl (pH 8.0), 300 mM NaCl, and 1 mM EDTA. The eluent was extracted twice in an equal volume of a 1:1 phenol/chloroform mixture and once with an equal volume of pure chloroform. The resulting RNAs in the aqueous phase were precipitated in 2.5 volumes of ethanol and recovered by centrifugation. RNA pellets were resuspended in 1 mL of glass-distilled water and dialyzed against 2 L of 1 mM EDTA overnight in a Float-A-lyzer G2 (Spectrum Laboratories) micro dialysis tube. RNAs were subsequently dialyzed against water for 24 h prior to storage at −20 °C.

Raman Spectroscopy. Raman spectra were recorded using a HoloLab Series 5000 Raman microscope (Kaiser Optical Systems). Individual samples (4 μL in the form of a hanging drop from a siliconized coverslip) were exposed to 100 mW of 647.1 nm laser excitation passed through the microscope's 20× objective lens for 300 s. Calibration of the Raman microscope was done using neon and tungsten lamp standards, which indicate that the variation in the positions of individual Raman bands is less than 1 cm^{-1}. The measurement of all spectra was conducted at ambient temperature, which varied between 20 and 25 °C. Variation of the Raman signals between 20 and 25 °C for the model compounds used in these studies was indistinguishable from the observed experimental error at constant temperature. Spectral data were analyzed using GRAMS/AI (Thermo Galactic Corp.). RNAs (20 mg/mL) and DMP (200 mM) were measured in 200 mM cacodylate (pH 6) in the absence or presence of different ions as indicated. ATP and ADP were measured at a reduced pH (3.8, 200 mM formate) to ensure a single negative charge per phosphate to parallel that of the other phosphodiesters compared in this work.

The effect of ion binding on the Raman signal for nonbridging phosphate oxygens was examined by quantitative analysis of Raman difference spectra in which the Raman spectrum of a phosphodiester model compound in the absence of ion (subtrahend) is subtracted from that in its presence (minuend).

Raman peaks that exhibited no detectable perturbation ($<2\%$) from ion binding were used as intensity standards that varied depending on the phosphodiester analyzed. Specifically, minuend and subtrahend spectra were normalized using the parent (raw) Raman peaks centered at 1466 and 1453 cm^{-1} for DMP, 842 cm^{-1} for ATP and ADP, 812 cm^{-1} for the GAAA tetraloop, and $\sim$726 cm^{-1} for all other RNAs. For ATP and all RNAs studied, the concentrations of the same samples used to generate minuend and subtrahend spectra were also analyzed by UV absorption in parallel to control for potential changes in concentration due to evaporation during Raman analysis. Magnesium hexahydrate [$Mg^{2+}(H_2O)_6$] was quantified from the intensity (photon counts) of the Raman peak for the $Mg^{2+}-O$ symmetric stretch ($\nu_s M-O$) centered at 360 cm^{-1} in the raw spectral data. Quantitative assessment of inner-sphere coordination was accomplished by measuring the observed Raman intensity in the positive node (PN) of the metal-induced inflection of $\nu_s PO_2^-$ in Raman difference spectra [$\nu_s PO_2^- M^{PN}$ (see the shaded region in the inset of Figure 2B)]. Raman difference spectra underestimate the total signal for $\nu_s PO_2^- M$ by $\sim$20% due the overlap of $\nu_s PO_2^-$ and $\nu_s PO_2^- M$ peaks in the Raman spectrum. The intensity of $\nu_s PO_2^- M^{PN}$, however, varies directly within experimental error with the total signal for $\nu_s PO_2^- M$ and allows a more accurate measure of changes in the Raman spectrum at lower concentrations of metal ion than peak fitting of small changes in the raw spectral data. All Raman difference spectra were derived from data collected during the same experiment.

Changes in the energetic difference between the Raman peaks for $\nu_s PO_2^-$ and $\nu_s PO_2^- M$ were monitored via the distance between the inflection points of the positive and negative nodes of the metal-induced inflection of $\nu_s PO_2^-$ in Raman difference spectra, which we define as $\Delta\nu M$ [$\Delta\nu M = \nu_s PO_2^- M - \nu_s PO_2^-$ (Figure 1D)]. Unlike the intensity of the positive node of the metal-induced inflection of $\nu_s PO_2^-$ in difference spectra, $\Delta\nu M$ overestimates the absolute difference between the peaks for $\nu_s PO_2^-$ and $\nu_s PO_2^- M$ due to their overlap in the Raman spectrum. Metal-induced changes in the position of $\nu_s PO_2^- M$ relative to $\nu_s PO_2^-$ are nevertheless reported directly through changes in the inflection points of the positive and negative nodes of the metal-induced inflection of $\nu_s PO_2^-$, yielding the value of $\Delta\nu M$. Measurement of $\Delta\nu M$ is thus utilized as a rapid means of comparing the relative differences in the spectroscopic position of $\nu_s PO_2^-$ and $\nu_s PO_2^- M$ due to the coordination of distinct metal ion species.

Data Analysis. The dependence of binding of Mg^{2+} to ATP and ADP was determined from the area of the positive peak of Raman difference spectra measured for ATP and ADP at different Mg^{2+} concentrations and plotted using a standard binding equation appropriate for approximately equal concentrations of metal ion and PO_2^- ligand:

$$ML = M_0 FA^{max}$$

$$= \left[L_0 + M_0 + K_d - \sqrt{(L_0 + M_0 + K_d)^2 - 4M_0 L_0} \right] \bigg/ 2$$

where ML is the concentration of bound ligand, FA^{max} is fraction of the maximum $\nu_s PO_2^- M$ signal observed, L_0 and M_0 are the initial concentrations of ligand and free metal, respectively, and K_d is the apparent dissociation constant. $M_0 FA^{max}$ values were normalized to unity to facilitate comparison. Areas of the positive peak of Raman difference spectra were determined using GRAMS/AI (Thermo Galactic Corp.). The experimental error
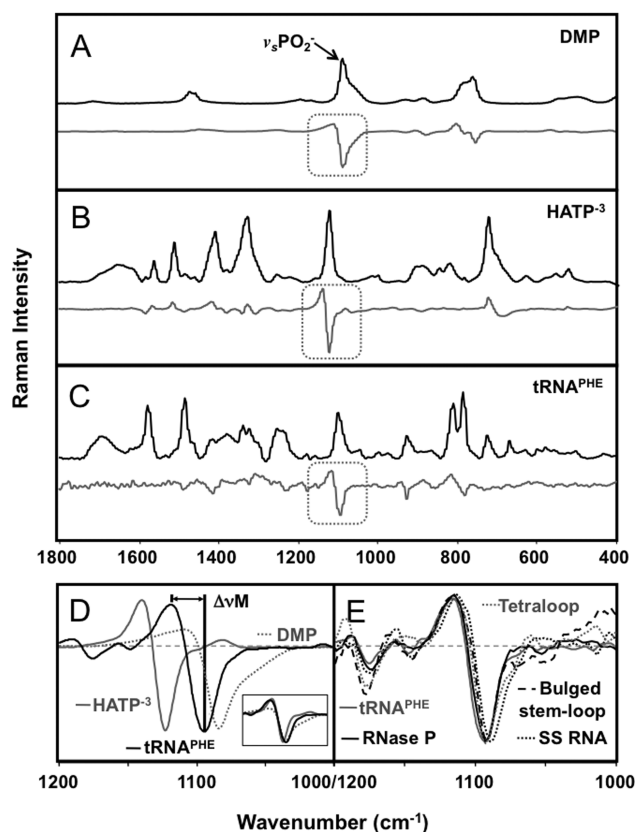

FIGURE 1: Effect of Mg^{2+} on the Raman spectra of structurally distinct phosphodiesters. Raman spectral data (black) and Raman difference spectra (subtracting spectra at 0 M from 0.3 M MgCl$_2$, dark gray) for 200 mM DMP (A), 100 mM HATP^{3-} (B), and 0.81 mM (20 mg/mL) yeast tRNA^{PHE} (C). (D) Overlay of Mg^{2+} difference spectra (1200$-$1000 cm^{-1}) of the symmetric stretch for nonbridging phosphate oxygens ($\nu_s PO_2^-$) for DMP (gray dots), HATP^{3-} (gray line), and yeast tRNA^{PHE} (black). The arrow indicates the spectral distance between inflection points of the positive and negative nodes (marked by vertical black lines) of the Mg^{2+}-induced inflection of $\nu_s PO_2^-$, which defines $\Delta\nu M$. The inset shows a superposition of the metal-induced inflections shown in panel D to illustrate the relative similarity in the apparent shift of $\nu_s PO_2^-$ to higher wavenumbers. (E) Overlay of Mg^{2+} difference spectra (1200$-$1000 cm^{-1}) of $\nu_s PO_2^-$ for an 11-nucleotide single-stranded RNA (black dots), 12-nucleotide GAAA tetraloop (gray dots), 27-nucleotide bulged stem$-$loop sequence (black dashes), 76-nucleotide yeast tRNA^{PHE} (dark gray line), and 400-nucleotide *E. coli* RNase P RNA (black line). Dotted gray boxes indicate the metal-induced inflection of $\nu_s PO_2^-$ observed in difference spectra. DMP and RNAs were measured at pH 6 (200 mM cacodylate), while HATP^{3-} was measured at pH 3.8 (200 mM formate) to generate a single negative charge on the terminal phosphate.

of reported peak areas or position reflects the observed variation from at least three independent experiments.

RESULTS

Contribution of Inner-Sphere, H-Bonding, and Electrostatic Interactions to Metal-Induced Changes in the Raman $\nu_s PO_2^-$ Signal of Phosphodiesters. Comparative studies of phosphodiester$-$ion interactions were performed using three model systems representing a range of structural complexity from a simple phosphodiester, dimethyl phosphate (DMP), to multiple adjacent phosphates, protonated ATP (HATP^{3-}, which maintains a single negative charge per phosphate), to a complex folded nucleic acid, yeast tRNA^{PHE} (Figure 1). In each case, $\nu_s PO_2^-$ is observed as a dominant spectroscopic feature at
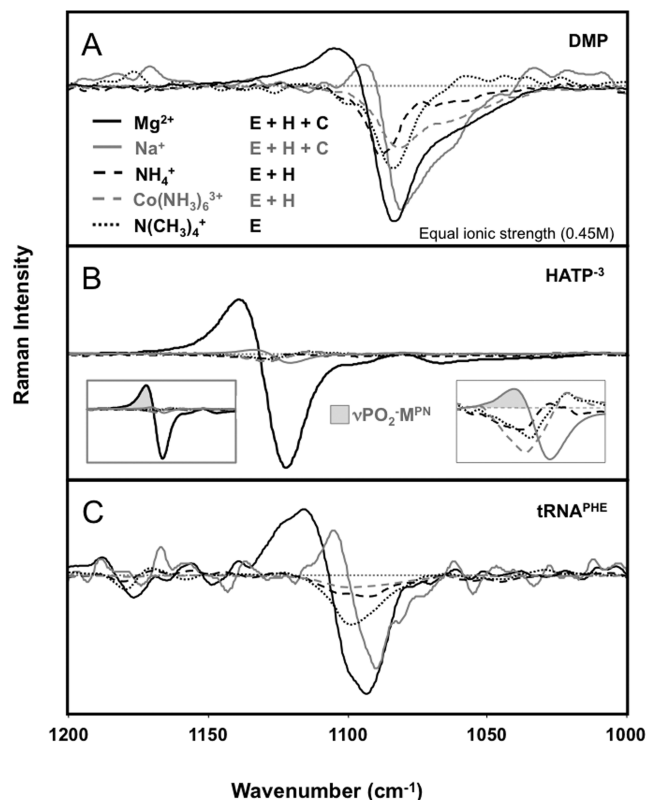
FIGURE 2: Influence of electrostatics, H-bonding, and inner-sphere coordination interactions on $\nu_s PO_2^-$. Raman difference spectra $(1200-1000~cm^{-1})$ of $\nu_s PO_2^-$ from DMP (A), HATP^{3-} (B), and yeast tRNA^{PHE} (C), in the presence of MgCl$_2$ (black line), NaCl (gray line), NH$_4$Cl (black dashed line), Co(NH$_3$)$_6$Cl$_3$ (gray dashed line), or N(CH$_3$)$_4$Cl (black dotted line) at an equal ionic strength of 0.45 M. The ability of individual metal ions to interact with nonbridging phosphate oxygens by electrostatic interactions (E), hydrogen bonding (H), or direct coordination (C) is noted by the aforementioned letters adjacent to the ions shown in the legend of panel A. The right inset in panel B shows an enlargement of all metal-induced difference spectra with the exception of that from MgCl$_2$ to facilitate comparison of weaker ion-induced changes to the Raman signal of HATP^{3-}. The left inset in panel B shows all metal-induced difference spectra, including that from MgCl$_2$. The shaded area in the positive node (PN) of metal ion difference spectra (Mg^{2+}, left inset; Na$^+$, right inset) reflects the shift of the $\nu_s PO_2^-$ signal to higher wavenumbers due to inner-sphere coordination defined by $\nu_s PO_2^-M^{PN}$. With the exception of metal ion concentration, experimental conditions are identical to those described in the legend of Figure 1.

approximately the same position ($\sim$1100 cm^{-1}) and is relatively isolated from other vibrational modes in the Raman spectrum of nucleic acids such as those from nucleotide bases ($\sim$1200–1500 cm^{-1}) or the ribose–phosphate backbone [$\sim$600–900 cm^{-1} (top black traces in Figure 1A–C)]. The strong similarity in these structurally distinct model systems is also observed for the intensity and shape of the $\nu_s PO_2^-$ peak. The observed $\nu_s PO_2^-$ signal thus is relatively insensitive to higher-order structure and is sufficient for quantitative analysis despite the relatively low signal-to-noise ratio compared to data obtained from crystals or surface-enhanced acquisition modes.

Metal-induced changes in the Raman spectrum were determined using difference spectra by subtraction of the spectrum of an individual phosphodiester from that in the presence of a metal ion (bottom gray traces, Figure 1A–C). When DMP, HATP^{3-}, and tRNA were examined at the same concentration of Mg^{2+} (0.3 M) in solution, metal-induced changes throughout their respective Raman difference spectra are readily observed.

Importantly, a similar metal ion-induced inflection near 1100 cm^{-1} is observed for each phosphodiester and is consistent with the apparent shift of $\nu_s PO_2^-$ to higher wavenumbers upon metal ion binding to form an altered vibrational mode ($\nu_s PO_2^-M$) as observed in previous solution and crystal studies (12–14, 16). In this comparison of Raman spectra at a constant concentration of Mg^{2+}, the total ionic strength (I) of the individual phosphodiesters was somewhat different (I^{DMP} = 1.1 M, I^{HATP} = 1.4 M, and I^{tRNA} = 1.1 M). Difference spectra compared at a constant ionic strength (Figure 2), however, are identical to those at a constant Mg^{2+} concentration.

An overlay of the Mg^{2+} difference spectra from DMP, HATP^{3-}, and yeast tRNA^{PHE} (Figure 1D) indicates that structural differences influence the position and amplitude of the observed inflection in the $\nu_s PO_2^-$ portion of the spectra (1095 ± 1, 1131 ± 1, and 1106 ± 2 cm^{-1} for DMP, HATP^{3-}, and yeast tRNA^{PHE}, respectively). Superposition of the difference spectra, however, shows that there is little difference in the degree of metal-induced displacement of $\nu_s PO_2^-$ to higher wavenumbers (inset in Figure 1D). The difference in the relative position of $\nu_s PO_2^-$ and $\nu_s PO_2^-M$ in the Raman spectrum defines the inflection points of the positive and negative nodes in the difference spectra. The apparent difference between the positive and negative nodes of difference spectra is defined as $\Delta\nu M$ [$\Delta\nu M = \nu_s PO_2^-M - \nu_s PO_2^-$ (Figure 1D)]. Because of a systematic error inherent to subtracting peaks with overlapping intensity, the apparent $\Delta\nu M$ overestimates the intrinsic difference between the $\nu_s PO_2^-$ and $\nu_s PO_2^-M$ peaks by $\sim$40%. Nonetheless, similar $\Delta\nu M$ values are observed for these structurally distinct phosphodiesters when they are compared using the same metal ion [$\Delta\nu M^{Mg}$ = 19 ± 1, 18 ± 1, and 24 ± 2 cm^{-1} for DMP, HATP^{3-}, and yeast tRNA^{PHE}, respectively (Figure 1D)]. This observation shows that structural differences have a much weaker effect on the differences in vibrational energy between $\nu_s PO_2^-M$ and $\nu_s PO_2^-$ than the energy of the $\nu_s PO_2^-$ vibration itself.

In addition to these model systems, we also compared the Mg^{2+} difference spectra of RNAs differing in structural complexity (Figure 1E). Specifically, we compared an unstructured RNA oligonucleotide (11 nucleotides) with four structured RNAs including a GAAA tetraloop (12 nucleotides), a bulged stem–loop structure derived from the P4 helix of RNase P RNA (20) (27 nucleotides), yeast tRNA^{PHE} (76 nucleotides, from Figure 1D), and the complete RNA subunit of *E. coli* RNase P (400 nucleotides). The metal-induced changes in $\nu_s PO_2^-$ for polynucleotides are almost identical in position, amplitude, and degree of displacement of $\nu_s PO_2^-$ to higher wavenumbers to form $\nu_s PO_2^-M$. The similarity of metal-induced changes in $\nu_s PO_2^-$ in these structurally distinct RNAs suggests that structural context has little effect on either $\nu_s PO_2^-$ or the formation of $\nu_s PO_2^-M$ in nucleic acids.

To determine the relative contribution of inner-sphere coordination, H-bonding, and electrostatic interactions to ion-induced changes in the $\nu_s PO_2^-$ region of the spectrum, we compared the Raman difference spectra of DMP, ATP, and yeast tRNA^{PHE} in the presence of metal and nonmetal ions that can interact variously via these three forms of chemical interaction (Figure 2). Specifically, we compared the effects of Mg^{2+} and Na$^+$, which can form both inner- and outer-sphere interactions with nonbridging phosphate oxygens, to that of exchange inert cobalt hexamine [Co(NH$_3$)$_6$$^{3+}$], a metal ion complex that mimics the overall structure of fully hydrated Mg^{2+} [Mg^{2+}(H$_2$O)$_6$] but is capable of only outer-sphere and electrostatic interactions (21).

In addition, we examined the effect of ammonium (NH_4^+) to monitor the influence of hydrogen bonding of an ion that differs from $Co(NH_3)_6^{3+}$ in size, charge, and geometry, as well as the effect of tetramethylammonium [$N(CH_3)_4^+$] to isolate electrostatic-induced changes in the νPO_2^- signal. To facilitate comparison of these distinct ions, we took initial measurements at equal ionic strengths (0.45 M). As expected from previous studies, ions capable of inner-sphere coordination (Mg^{2+} and Na^+) produced characteristic inflections of $\nu_s PO_2^-$ in the Raman difference spectrum in DMP, ATP, and tRNA (Figure 2). In contrast, however, we found that ions restricted to outer-sphere and/or electrostatic interactions [$Co(NH_3)_6^{3+}$, NH_4^+, or $N(CH_3)_4^+$] resulted only in the attenuation of the $\nu_s PO_2^-$ Raman signal near 1100 cm^{-1}.

Differences in the relative amplitude of Mg^{2+}- and Na^+-induced changes in $\nu_s PO_2^-$ in different model compounds appear to reflect differences in the relative affinity of individual ions. The Na^+-induced changes in the $\nu_s PO_2^-$ region of the spectra of ATP are significantly smaller than those observed for Mg^{2+}. ATP forms a tight ($K_d \sim 10^{-5}$ M) stoichiometric complex with Mg^{2+} via interactions involving one or more of the phosphate oxygens, which strongly favors binding of the divalent ion (*22−24*). In contrast, Na^+-induced inflections of $\nu_s PO_2^-$ were found to be nearly equal in magnitude to that of Mg^{2+} in DMP and only somewhat reduced in magnitude relative to the magnitude of changes in the spectrum due to Mg^{2+} in the context of yeast tRNA^{PHE}, where only a few of the nonbridging phosphate oxygens are involved in site-specific divalent metal ion binding.

The absence of the induction of the $\nu_s PO_2^- M$ vibrational mode by $Co(NH_3)_6^{3+}$, NH_4^+, or $N(CH_3)_4^+$ is consistent with their inability to form inner-sphere coordination interactions with phosphodiesters. Alternatively, the same negative result could be due to low relative affinities of these ions for diesters, nucleotides, and nucleic acids relative to Na^+ and Mg^{2+}. Cobalt hexamine, however, binds to nucleic acids with affinities similar to that observed for Mg^{2+} (*25*). To test whether this is the case under our experimental conditions, we measured the intensity (photon counts) of the positive node (PN) of the metal-induced HATP^{3-} $\nu_s PO_2^-$ difference spectra [$\nu_s PO_2^- M^{PN}$ (shaded area in in the inset of Figure 2B)] as a function of Mg^{2+} concentration in the presence and absence of $Co(NH_3)_6^{3+}$ (Figure S1 of the Supporting Information). We find that $Co(NH_3)_6^{3+}$ can compete with Mg^{2+} for ATP binding with a concentration dependence that indicates a similar affinity. Binding of $Co(NH_3)_6^{3+}$ is also implied by the attenuation of $\nu_s PO_2^-$ in the presence of $Co(NH_3)_6^{3+}$ alone (Figure 2B). Indeed, for all phosphodiesters tested to date, binding of $Co(NH_3)_6^{3+}$ results in attenuation of the intensity of the Raman signal from the $\nu_s PO_2^-$ vibrational mode without formation of the $\nu_s PO_2^- M$ mode associated with inner-sphere coordination (E. L. Christian, unpublished observations). Similarly, $\nu_s PO_2^-$ attenuation in the absence of formation of $\nu_s PO_2^- M$ is observed in the presence of NH_4^+ or $N(CH_3)_4^+$ at an ionic strength equivalent to that examined for $MgCl_2$ [450 mM (Figure 2)] and near the limit of NH_4^+ solubility [4 M (data not shown)]. Thus, the ion-induced attenuation of $\nu_s PO_2^-$ appears to result from electrostatic interactions, H-bonding, and likely inner-sphere coordination, while the formation of $\nu_s PO_2^- M$ reflects purely inner-sphere coordination.

Testing the Dependence of $\nu_s PO_2^- M$ on Inner-Sphere Coordination by a Metal Ion Specificity Switch. To further understand the chemical basis for the attenuation of $\nu_s PO_2^-$ and formation of $\nu_s PO_2^- M$, we compared the Raman spectra of
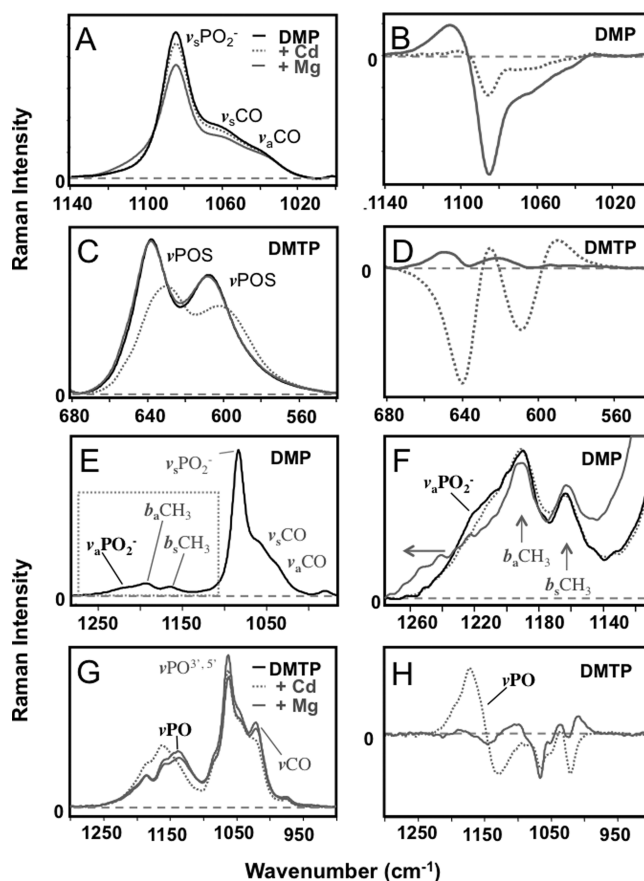

FIGURE 3: Dependence of $\nu_s PO_2^- M$ on direct metal ion coordination. (A) Raman spectrum (1140−1000 cm^{-1}) of $\nu_s PO_2^-$ from 0.2 M DMP in the absence of metal (black) or presence of 1 M Mg^{2+} (gray dots) or 1 M Cd^{2+} (gray line). (B) Difference spectrum subtracting DMP in the absence of metal from that in the presence of 1 M Mg^{2+} (gray line) or 1 M Cd^{2+} (dark gray). (C) Raman spectrum (680−540 cm^{-1}) of isolated νPOS^- from 0.2 M DMTP in the absence of metal (black) or presence of 1 M Mg^{2+} (light gray) or 1 M Cd^{2+} (dark gray). (D) Difference spectrum subtracting DMTP in the absence of metal from that in the presence of Mg^{2+} (light gray) or 1 M Cd^{2+} (dark gray). (E) Raman spectrum (1300−950 cm^{-1}) showing both symmetric ($\nu_s PO_2^-$) and asymmetric ($\nu_a PO_2^-$) stretches for nonbridging phosphate oxygens from 0.2 M DMP in the absence of metal (black) or presence of 1 M Mg^{2+} (light gray) or 1 M Cd^{2+} (dark gray). (F) Enlargement of the region of the Raman spectrum shown as a dotted box in panel E showing DMP in the absence of metal ion (black) or in the presence of 1 M Mg^{2+} (light gray) or 1 M Cd^{2+} (dark gray). The assignments of $\nu_s PO_2^-$, νPOS^-, and νPO have been previously established in the literature (*27, 43*), and their associated metal-dependent shifts were confirmed by ^{18}O substitution (data not shown). (G) Raman spectrum (1300−900 cm^{-1}) near the phosphoryl vibrational mode (νPO) from 0.2 M DMTP in the absence of metal (black) or presence of 1 M Mg^{2+} (light gray) or 1 M Cd^{2+} (light gray). Additional peaks of bridging O−P−O ($\nu PO^{3'5'}$) and C−O stretch (νCO) are shown for reference. (H) Difference spectrum of the region shown in panel G subtracting DMTP in the absence of metal from that in the presence of 1 M Mg^{2+} (light gray) or 1 M Cd^{2+} (dark gray). Additional vibrational modes in DMP and DMTP are provided for reference: $\nu_s CO$ and $\nu_a CO$ reflect the symmetric and asymmetric C−O stretch, respectively, and $b_s CH_3$ and $b_a CH_3$ reflect the symmetric and asymmetric bending modes of the methyl group, respectively (*27, 43*).

dimethyl phosphate (DMP) and dimethyl thiophosphate (DMTP) in the presence of either an oxophilic ion, Mg^{2+}, or a thiophilic ion, Cd^{2+} (Figure 3). It is well-established that sulfur substitution of a nonbridging phosphate oxygen strongly inhibits inner-sphere coordination of oxophilic ions such as Mg^{2+} (31000-fold

preference for oxygen over sulfur in ATPβS) but allows inner-sphere coordination of thiophilic ions such as Cd^{2+} (60-fold preference for sulfur over oxygen in ATPβS) (*22, 23, 26*). Thus, the extent to which Mg^{2+} and Cd^{2+} induce changes in the Raman spectrum of DMP and DMTP should provide an additional test for the linkage among inner-sphere coordination, attenuation of $\nu_sPO_2^-$, and formation of $\nu_sPO_2^-M$.

In contrast to the strong Mg^{2+}-induced attenuation of $\nu_sPO_2^-$ and formation of $\nu_sPO_2^-M$ in the Raman difference spectrum of DMP, similar spectral changes are not induced by Mg^{2+} in the corresponding νPOS^- vibrational mode in DMTP, shown in previous studies to form two characteristic signals at 607 and 638 cm^{-1} (*27*) and confirmed in the current work by ^{18}O substitution (data not shown) (compare panels A and B of Figure 3 with panels C and D). Significant attenuation of the intensity of the νPOS^- modes in DMTP, however, is observed in the presence of Cd^{2+}, but not for $\nu_sPO_2^-$ in DMP. In addition, new metal ion-dependent vibrational modes are observed down-field from the unperturbed νPOS^- in the presence of Cd^{2+}, while no significant $\nu_sPO_2^-M$ formation is evident in DMP. Consistent with the observations described above, Ca^{2+} and Mn^{2+}, which show a strong preference for oxygen over sulfur (31000–39000- and 158–193-fold, respectively, in ATPβS), also produce metal-dependent shifts and attenuation of $\nu_sPO_2^-$ of DMP but not DMTP, while Co^{2+} and Zn^{2+}, which have been shown to have only a weak preference for sulfur over oxygen ($\sim$1.2- and 4.6-fold, respectively, in AMPS), produce metal-dependent shifts and attenuation of $\nu_sPO_2^-$ in both DMP and DMTP (*22, 28*).

Metal ion specificity is also evident in the vibrational modes coupled to $\nu_sPO_2^-$ and νPOS^-. In DMP, metal ion coordination is predicted to alter the asymmetric ($\nu_aPO_2^-$) and symmetric ($\nu_sPO_2^-$) vibrational modes of the nonbridging phosphate oxygens because the atoms involved are identical. Consistent with this prediction, $\nu_aPO_2^-$ is shifted to higher wavenumbers in the presence of Mg^{2+}, but not in the presence of Cd^{2+} (Figure 3E,F). Similarly, in DMTP, metal ion coordination to sulfur is predicted to alter the bond order and vibrational properties of the phosphoryl (P=O, νPO) as well as the adjacent P–S bond since these vibrational modes share the same phosphorus atom. Indeed, significant perturbation of νPO is observed for DMTP in the presence of Cd^{2+}, but not in the presence of Mg^{2+} (Figure 3G,H). Taken together, the dependence of the metal-induced shift of $\nu_sPO_2^-$, νPOS^-, and their coupled vibrational modes on oxophilic or thiophilic ions strongly supports the interpretation that these spectroscopic signals arise from direct inner-sphere coordination, consistent with the findings described above.

Thermodynamic Relationship between Saturable Ion Binding and $\nu_sPO_2^-M$. The utility of $\nu_sPO_2^-M$ as a quantitative probe for inner-sphere coordination interactions is directly related to the extent to which this spectroscopic feature can be used to accurately measure metal binding thermodynamics. A simple and well-characterized system for studying inner-sphere metal ion binding is provided by $HATP^{3-}$ which binds a single Mg^{2+} with high affinity through interactions with the nonbridging phosphate oxygens and maintains a single negative charge per phosphodiester (*22–24*). We therefore determined the extent to which increasing concentrations of Mg^{2+} resulted in concentration-dependent and saturable changes in the intensity of $\nu_sPO_2^-M^{PN}$. We also compared changes in $\nu_sPO_2^-M^{PN}$ to the intensity of the Raman signal for magnesium hexahydrate [$Mg^{2+}(H_2O)_6$] which can be detected by its symmetric stretching

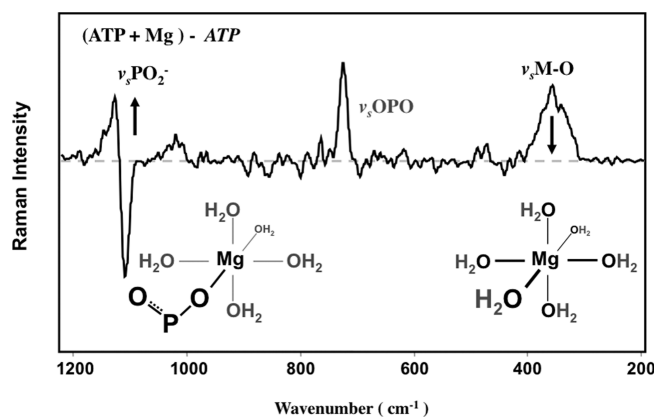FIGURE 4: Inner-sphere coordination induces $\nu_sPO_2^-M$ formation and ν_sM-O attenuation. Raman difference spectrum of ATP (60 mM) in the presence of excess $MgCl_2$ (200 mM), indicating the relative positions of the Mg^{2+}-induced changes in $\nu_sPO_2^-$ ($\sim$1100 cm^{-1}) and magnesium hexahydrate (ν_sM-O, 360 cm^{-1}, structure at the right). Black arrows reflect previously observed correlations of Mg^{2+} binding (structure at the left) with an increased $\nu_sPO_2^-$ inflection and a decreased ν_sM-O intensity in DMP solution studies and crystals of the HDV ribozyme (*12*).

frequency at 360 cm^{-1} [ν_sM-O (Figure 4)]. As noted above, loss of the Raman signal for fully hydrated magnesium and formation of magnesium penta- or tetrahydrate have been shown to correlate with increases in the intensity of $\nu_sPO_2^-M$ in DMP and crystals of HDV ribozyme RNA (*12*). If $\nu_sPO_2^-M$ represents stoichiometric binding of Mg^{2+} to ATP in a site-bound or chelated mode, then its intensity should follow predictable saturation binding thermodynamics with respect to Mg^{2+} concentration. In addition, inner-sphere coordination of Mg^{2+} by ATP must necessarily lead to a stoichiometric decrease in ν_sM-O.

As shown in Figure 5, saturable binding behavior can be observed in the Mg^{2+} concentration dependence of the intensity of $\nu_sPO_2^-M^{PN}$ under conditions where the ionic strength varies with the concentration of the added metal ion. Importantly, the apparent equilibrium constant for the $Mg^{2+}-HATP^{3-}$ complex determined by measuring $\nu_sPO_2^-M^{PN}$ (log $K^a = 2.8 \pm 1.0$ M^{-1}) is equal to that observed by NMR under similar conditions (log $K^a = 2.79 \pm 0.15$ M^{-1}) (*22*). Furthermore, because the nucleotide concentration is in excess of the dissociation constant for Mg^{2+} ion binding, the stoichiometry for ion binding detected by $\nu_sPO_2^-M^{PN}$ can be estimated from the intersection of lines tangent to the initial and saturating phases of the binding curve. The intersection observed for ATP–Mg^{2+} binding extrapolates to 100 mM $MgCl_2$ on the x-axis (Figure 4A), and the apparent stoichiometric ratio of 100 mM Mg^{2+} to 300 mM phosphate or 100 mM ATP is consistent with the binding of a single metal ion by ATP as observed in previous studies.

To test whether the metal dependence of $\nu_sPO_2^-M^{PN}$ intensity was specific to the nonbridging phosphate oxygens and distinguishable from metal-dependent changes in other vibrational modes in the Raman spectrum, we monitored Mg^{2+}-dependent changes in the vibrational modes of the adenine base. Base vibrational modes are significantly more sensitive to metal-induced changes in geometry than $\nu_sPO_2^-$ (*13*). Indeed, as shown in Figure 1B, the presence of Mg^{2+} produces significant perturbation of the adenosine ring of ATP modes between 1200 and 1500 cm^{-1} in the Raman spectrum. Previous studies show that Mg^{2+} binding to ATP and ADP can involve simultaneous
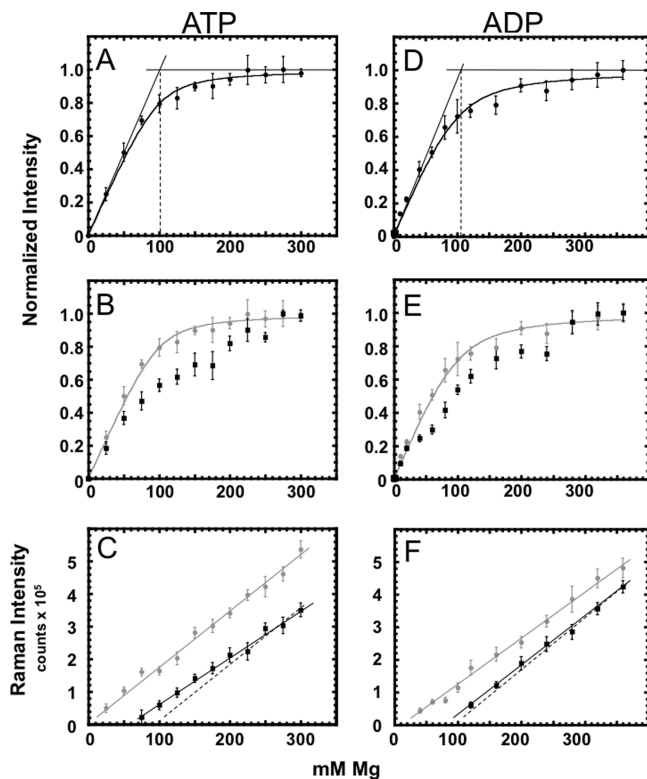
FIGURE 5: Use of $\nu_sPO_2^-M^{PN}$ to monitor site-specific metal ion binding. (A) Dependence of 100 mM protonated ATP ($HATP^{3-}$) $\nu_sPO_2^-M^{PN}$ on $MgCl_2$ concentration (millimolar). Black circles reflect the normalized upshifted $\nu_sPO_2^-$ Raman signal (photon counts) derived from the positive node of the Raman difference spectra ($\nu_sPO_2^-M^{PN}$). The black curve reflects the fit of $\nu_sPO_2^-M^{PN}$ data to the binding isotherm appropriate for approximately equal concentrations of $HATP^{3-}$ and $MgCl_2$ (see Methods). Solid black lines reflect tangents to the initial and saturating phases of the binding curve. The dotted black line reveals the $MgCl_2$ concentration corresponding to the intersection of tangent lines above and the stoichiometry of Mg^{2+} binding to $HATP^{3-}$. (B) Dependence of the $HATP^{3-}$ adenine Raman peak at 1310 cm^{-1} (νA_{1310}) on $MgCl_2$ concentration. Black squares reflect the normalized upshifted νA_{1310} Raman signal derived from the positive node of the Raman difference spectra (νA_{1310}^{PN}). The gray ovals and curve reflect the normalized Mg^{2+} dependence of the increase in $\nu PO_2^-M^{PN}$ as described for panel A. (C) Dependence of the Raman peak for fully hydrated Mg^{2+} [$Mg(H_2O)_6^{2+}$, $\nu Mg-O$, 360 cm^{-1}] on Mg^{2+} concentration in the absence (gray) and presence of 100 mM $HATP^{-3}$ (black). Solid lines reflect the linear least-squares fit to all points in the absence (gray) or presence (black) of $HATP^{3-}$. Dotted lines reflect the least-squares fit to points above 200 mM $MgCl_2$, where Mg^{2+} binding to $HATP^{3-}$ is observed to be saturating. (D–F) Repeats of experiments depicted in panels A–C, respectively, but in the presence of 100 mM protonated ADP ($HADP^{2-}$). Protonated forms of ATP and ADP were chosen to parallel the single negative charge per phosphate of the other phosphodiesters compared in this work.

inner-sphere coordination with nonbridging phosphate oxygens and outer-sphere coordination with N7 of adenine, which raises the possibility of coupled metal ion dependence for the vibrational modes associated with these two functional groups (29−32). We therefore measured the positive node of the metal-induced shift in the Raman signal for the adenine ring mode at ∼1310 cm^{-1} for ATP (νA_{1310}^{PN}) as a function Mg^{2+} concentration and compared it to that observed for $\nu_sPO_2^-M^{PN}$ (Figure 5B). Changes in the intensity of νA_{1310}^{PN} as a function of Mg^{2+} concentration are clearly distinct from that observed for $\nu_sPO_2^-M^{PN}$. In contrast to the saturable binding behavior of $\nu_sPO_2^-M^{PN}$, the metal-dependent change in νA_{1310}^{PN} intensity

shows at least two distinct phases with no sign of apparent saturable binding behavior over the same Mg^{2+} concentration range. Metal-dependent changes in $\nu_sPO_2^-M^{PN}$ thus are only weakly coupled to changes in the adenosine base, and quantification of its intensity allows isolation of metal ion interactions of the nonbridging phosphate oxygens.

To further test the extent to which $\nu_sPO_2^-M^{PN}$ correlates quantitatively with inner-sphere metal ion coordination, we determined the concentration dependence of the intensity of the Raman peak for fully hydrated Mg^{2+} (ν_sM-O) in the absence and presence of 100 mM ATP (Figure 5C). The high concentration of ATP relative to the dissociation constant for Mg^{2+} ensures that essentially all metal ions are bound at substoichiometric concentrations (e.g., <50 mM) of Mg^{2+}. Under these conditions ν_sM-O is readily and quantitatively detected in the absence of ATP. However, in the presence of 100 mM ATP, the expected linear increase in ν_sM-O is shifted to higher $MgCl_2$ concentrations with an x-axis intercept between 50 and 100 mM Mg^{2+}. These data show that fully hydrated Mg^{2+} is undetectable between 0 and 50 mM $MgCl_2$ in the presence of 100 mM ATP, the same concentration range over which the intensity of $\nu_sPO_2^-M^{PN}$ has an essentially linear concentration dependence. The x-axis intercept between 50 and 100 mM Mg^{2+} observed for ν_sM-O in the presence of 100 mM ATP also provides further evidence of a 1:1 stoichiometry of the $Mg^{2+}-ATP$ complex (22−24).

Previous isotope (^{18}O) substitution experiments designed to detect interactions with individual phosphate oxygens in ATP indicate that metal ion binding α-, β-, or γ-phosphates all participate in the formation of the $\nu_sPO_2^-M$ vibrational mode (33). Metal complexes with ATP, however, include a mixture of mono- or multidentate (α−β, β−γ, or α−β−γ) phosphate−metal complexes in which individual $\nu_sPO_2^-M$ vibrational modes are likely to be coupled (33). This observation raises the possibility that the complexity of phosphate−metal complexes in ATP might preclude the use of this model system to monitor metal-dependent changes in $\nu_sPO_2^-$. To examine the extent to which complex heterogeneity and vibrational mode coupling affect the observed metal-dependent changes in $\nu_sPO_2^-M^{PN}$ seen in site-specific ion binding, we repeated the Mg^{2+} titration studies above using the proton form of ADP ($HADP^{2-}$) (Figure 5D−F). $HADP^{2-}$ forms a more structurally homogeneous population with metal contacts to both α- and β-phosphates at sufficient affinity (log K^a = 2.94 ± 0.14 M^{-1}) to allow stoichiometric binding of Mg^{2+} (22). Increasing concentrations of Mg^{2+} resulted in an increasing intensity of $\nu_sPO_2^-M^{PN}$ that followed saturable binding and stoichiometric behavior analogous to that observed for ATP (Figure 5D). The saturable binding behavior of ADP $\nu_sPO_2^-M^{PN}$ is clearly distinct from the metal ion concentration-dependent changes in the Raman signal for the adenosine base at ∼1310 cm^{-1} [νA_{1310}^{PN} (Figure 5E)]. We also find that fully hydrated Mg^{2+} is undetectable between 0 and 50 mM $MgCl_2$ in the presence of 100 mM ADP, the same concentration range over which the intensity of metal-induced $\nu_sPO_2^-M^{PN}$ in ADP has an essentially linear concentration dependence (Figure 5D,F). Different mixtures of mutidentate phosphate−metal complexes that likely include different degrees of vibrational coupling between phosphates thus do not appear to contribute significantly to the observed metal-dependent changes in the Raman spectrum of ATP and ADP. Together, these data strongly support the interpretation that inner-sphere coordination between metal ion and nonbridging oxygen can be
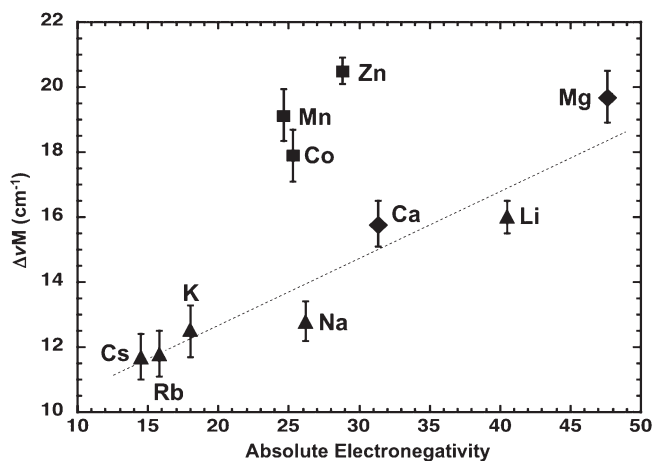
FIGURE 6: Dependence of $\Delta\nu$M on absolute electronegativity. Magnitudes of the metal-induced shift of ν_sPO$_2^-$ to higher wavenumbers ($\Delta\nu$M) of 0.2 M DMP in the presence of alkali (▲), alkaline earth (◆), and transition (■) metals at equal ionic strengths (3 M) plotted vs measured values of metal ion absolute electronegativity as reported by Pearson (*34*).

quantified by integration of the intensity of ν_sPO$_2^-$M^{PN} and that this signal is likely to be applicable to the solution analysis phosphodiesters in general.

Effects of Ion Identity on ν_s*PO$_2^-$ M.* The thermodynamic correlations between the intensity of ν_sPO$_2^-$M^{PN} and metal ion binding via inner-sphere coordination interactions predict that this spectroscopic signal should be strongly influenced by the physical properties of different metal ions. Absolute electronegativity reflects an atom's ability to attract electrons toward itself in a chemical bond and therefore is likely to strongly correlate with the vibrational properties of ν_sPO$_2^-$M (*34*). We therefore measured the degree of the ν_sPO$_2^-$ shift to higher wavenumbers ($\Delta\nu$M) reflected in the metal-induced inflection observed in Raman difference spectra of DMP in the presence of different metal ions at a constant (3 M) ionic strength (Figure 6). Examples of individual metal-induced changes to ν_sPO$_2^-$ in DMP Raman spectra are shown in Figures S2 and S3 of the Supporting Information.

When $\Delta\nu$M (in cm^{-1}) is plotted as a function of absolute electronegativity, the behavior of individual ions falls into two groups. Alkali and alkaline earth metals show a linear dependence of the magnitude of $\Delta\nu$M on electronegativity, while transition metals do not follow this trend (Figure 6). Two transition metals (Cd^{2+} and Ni^{2+}) produced no significant ν_sPO$_2^-$ shift to higher wavenumbers, presumably due to low levels of inner-sphere coordination to DMP (data not shown). The same distinction between types of metal ions is observed when $\Delta\nu$M is plotted versus the related physical property of absolute hardness (Figure S4 of the Supporting Information). In the current analysis of the comparison of $\Delta\nu$M values for different metal ions at constant ionic strengths, the metal: phosphodiester molar ratio will differ by approximately 3-fold between mono- and divalent metal ions. The parameter $\Delta\nu$M, however, is essentially insensitive to differences in the metal: phosphodiester molar ratio as no significant change in $\Delta\nu$M is observed over a broad ion concentration range (e.g., 1−5 M Na$^+$ or 0.15−2 M Mg^{2+}) for all metal ions shown in Figure 6 (Figure S5 of the Supporting Information). A linear fit of $\Delta\nu$M as a function of metal ion concentration yields little to no slope, indicating that the metal-induced shifts of ν_sPO$_2^-$, and thus

Table 1: Effect of Structure on $\Delta\nu$M^a

model system	no. of nucleotides	$\Delta\nu$M for Na$^+$	$\Delta\nu$M for Mg^{2+}
DMP		12.8 ± 0.6	19.7 ± 0.8
ATP	1	13 ± 1	18 ± 1
single-stranded RNA	11	16 ± 3	24 ± 2
GAAA tetraloop	12	18 ± 2	25 ± 2
P4 hairpin	27	15 ± 3	23 ± 2
yeast tRNA^{PHE}	76	16 ± 2	24 ± 2
RNase P RNA	400	16 ± 3	24 ± 2

^{a}Measured $\Delta\nu$M induced by Na$^+$ (3 M) or Mg^{2+} (1 M) in 0.2 M DMP, 100 mM ATP, or 20 mg/mL 11-nucleotide single-stranded RNA (ssRNA), 27-nucleotide RNA hairpin from the P4 NMR fragment of RNase P RNA (*20*), 76-nucleotide yeast tRNA^{PHE}, or 400-nucleotide RNase P RNA. All samples were analyzed as described in the legend of Figure 1.

$\Delta\nu$M, reflect distinct physical properties of the individual metal−phosphate interactions. In particular, the data given above indicate for alkali and alkaline earth metals, and thus many of the metals used in the study of phosphodiester chemistry and nucleic acids structure, that absolute electronegativity and absolute hardness contribute significantly to the vibrational energy of ν_sPO$_2^-$M and are strong predictors of the observed degree of the ν_sPO$_2^-$ shift to higher wavenumbers.

The differences in the magnitude of $\Delta\nu$M for different metal ions relative to the observed experimental error ($\leq$1 cm^{-1}) suggest that this physical parameter could be used to identify or distinguish between individual metal ion species. Na$^+$ and Mg^{2+}, for example, are clearly resolved in the structurally distinct model systems of DMP ($\Delta\nu$M^{Na} = 12.8 ± 0.6 cm^{-1}, and $\Delta\nu$M^{Mg} = 19.7 ± 0.8 cm^{-1}), ATP ($\Delta\nu$M^{Na} = 13 ± 1 cm^{-1}, and $\Delta\nu$M^{Mg} = 18 ± 1 cm^{-1}), and yeast tRNA^{PHE} ($\Delta\nu$M^{Na} = 16 ± 2 cm^{-1}, and $\Delta\nu$M^{Mg} = 24 ± 2 cm^{-1}) (Figure 2A−C). We therefore further tested the generality of this effect by measuring the extent to which Na$^+$ and Mg^{2+} binding could still be resolved in RNAs differing in complexity. Table 1 compares $\Delta\nu$M induced by Na$^+$ and Mg^{2+} in DMP and ATP with that observed in a single-stranded RNA oligonucleotide (11 nucleotides), a GAAA tetraloop (12 nucleotides), a bulged stem−loop structure (27 nucleotides), yeast tRNA^{PHE} (76 nucleotides), and *E. coli* RNase P RNA (400 nucleotides). We find that the ability to distinguish $\Delta\nu$M values induced by Na$^+$ from that induced Mg^{2+} is maintained in all model systems tested. Although the magnitude of the difference in the $\Delta\nu$M induced by Na$^+$ relative to Mg^{2+} is somewhat variable between different model compounds, this difference is well within the magnitude of the somewhat larger experimental error ($\sim$2−3 cm^{-1}) observed for RNA samples (Table 1). These data indicate that $\Delta\nu$M is likely to be broadly useful for the characterization or distinction between individual metal ion species interacting with the phosphoryl oxygens of nucleotides, nucleic acids, and other phosphodiester model compounds.

DISCUSSION

Metal-induced changes to the symmetric stretch of nonbridging phosphate oxygens in the Raman spectrum (ν_sPO$_2^-$) have long been used as an experimental signal for metal binding in phosphodiester model compounds and nucleic acids and have recently been proposed as a semiquantitative measure of inner-sphere coordination (*12−15, 33*). Missing from current methods, however, is an understanding of the extent to which phosphodiester structure and indirect forms of metal ion interaction such

as H-bonding and electrostatic effects contribute to the observed metal-dependent changes in the Raman spectra of phosphodiesters. Such an understanding is necessary for quantitative interpretation of the Raman spectra in terms of ion interactions. In this work, we find that the attenuation of $\nu_s PO_2^-$ is due to all three forms of chemical interaction, while the characteristic shift of $\nu_s PO_2^-$ to higher wavenumbers in Raman difference spectra can be induced only by ions capable of inner-sphere coordination of the nonbridging phosphoryl oxygens. We also show that the shift of $\nu_s PO_2^-$ to higher wavenumbers is dependent on metal ion identity and may be used to estimate the distribution of ions binding in mixed metal ion solutions. These findings are observed in structurally distinct model compounds and thus appear to reflect the spectroscopic behavior of metal ion binding to phosphodiesters in general.

The observations described above provide insight into the physical basis for differences in the metal-dependent changes in $\nu_s PO_2^-$ by different metal ions in difference spectra from different phosphodiester model systems. In DMP, which lacks the structural complexity to form high-affinity complexes with individual ions, the extent of formation of $\nu_s PO_2^- M^{PN}$ induced by Mg^{2+} is only severalfold larger than that induced by Na^+, while the extents of attenuation of $\nu_s PO_2^-$ induced by Mg^{2+} and Na^+ are essentially equal (Figure 2A). Attenuation induced by Co-$(NH_3)_6^{3+}$ and NH_4^+ (H-bonding) and $N(CH_3)_4^+$ (electrostatic interactions) are roughly equal in intensity with each other and are approximately half the intensity induced by Mg^{2+} or Na^+. Although quantitative comparison of weakly bound ion pairs is problematic, qualitatively these data show that for a single phosphodiester ion-induced changes in $\nu_s PO_2^-$ can involve both shifts to higher wavenumbers from inner-sphere coordination and significant attenuation by electrostatic (and possibly H-bonding) interactions. The data also suggest that the relative contributions of direct and indirect interactions from Mg^{2+}- and Na^+-induced changes in $\nu_s PO_2^-$ are not equal. While similar levels of Mg^{2+}- and Na^+-induced attenuation of $\nu_s PO_2^-$ reflect similar total levels of metal−phosphate interaction with DMP, a proportionally higher intensity of $\nu_s PO_2^- M^{PN}$ induced by Mg^{2+} suggests a greater fraction of inner-sphere coordination interactions than that with Na^+.

Differences in the relative contribution of inner-sphere versus H-bonding/electrostatic interactions are increased dramatically in the context of the high-affinity Mg^{2+} binding site created by $HATP^{3-}$, where Mg^{2+}-induced formation of $\nu_s PO_2^- M^{PN}$ and attenuation of $\nu_s PO_2^-$ dwarf those observed by other ions (Figure 2B). In addition, the intensity of Mg^{2+}-induced $\nu_s PO_2^- M^{PN}$ relative to attenuation of $\nu_s PO_2^-$ is much larger than that observed in DMP. These data reveal significantly enhanced levels of inner-sphere coordination in the context of site-specific binding relative to that observed for an unstructured phosphodiester. In contrast, the relative levels of ion-induced changes caused by Na^+, $Co(NH_3)_6^{3+}$, NH_4^+, and $N(CH_3)_4^+$ in ATP are roughly similar to those observed in DMP (Figure 2B, right inset). The level of Na^+-induced $\nu_s PO_2^- M^{PN}$ induction relative to $\nu_s PO_2^-$ attenuation is nevertheless significantly larger in ATP than that observed in DMP, indicating a greater degree of inner-sphere coordination in the context of the polyphosphate. Similarly, the level of attenuation of $\nu_s PO_2^-$ by $Co(NH_3)_6^{3+}$ is nearly equal to or somewhat reduced relative to that observed for NH_4^+, and $N(CH_3)_4^+$ in DMP, but larger than the observed levels of $\nu_s PO_2^-$ attenuation by NH_4^+, and $N(CH_3)_4^+$ in ATP, consistent with the

measured similarity of Mg^{2+} and $Co(NH_3)_6^{3+}$ binding to ATP observed in the competition studies described above (Figure S1 of the Supporting Information).

Interestingly, ion-dependent changes in $\nu_s PO_2^-$ in yeast $tRNA^{PHE}$ indicate enhanced levels of inner-sphere metal ion coordination relative to DMP (compare panels A and C of Figure 2). Specifically, the intensity of Mg^{2+}-induced $\nu_s PO_2^- M^{PN}$ relative to attenuation of $\nu_s PO_2^-$ is much larger than that observed in DMP and is likely to reflect a higher binding free energy due to the higher charge density of the polyanion. Alternatively, the greater intensity of $\nu_s PO_2^- M^{PN}$ for $tRNA^{PHE}$ could correlate with site-specific metal ion binding. However, the same ratio of $\nu_s PO_2^- M^{PN}$ to $\nu_s PO_2^-$ attenuation is observed for a short (11-nucleotide) single-stranded RNA oligonucleotide and other structurally distinct RNAs (Figure 1E). The insensitivity of the ratio of $\nu_s PO_2^- M^{PN}$ to $\nu_s PO_2^-$ between $tRNA^{PHE}$ and different RNA structures suggests that $\nu_s PO_2^- M^{PN}$ largely reflects diffuse metal ion binding. Consistent with this observation, the relative intensities of $\nu_s PO_2^- M^{PN}$ induced by Mg^{2+} and Na^+ in $tRNA^{PHE}$ are similar to that observed for DMP (Figure 2A) despite multiple site-bound Mg^{2+} ions in $tRNA^{PHE}$ that will be fully occupied at 150 mM Mg^{2+} (*35−37*). The data described above suggest that diffuse interactions by mono- and divalent metal ions in nucleic acids are also involved in low but measurable levels of inner-sphere coordination. Thus, while important qualitative information can be gained by analysis of changes in $\nu_s PO_2^- M^{PN}$ for RNA, significant additional investigation will be necessary to understand how to interpret these data quantitatively.

Nonetheless, the data presented here provide insight into the physical basis of the shift of $\nu_s PO_2^-$ to higher wavenumbers to form $\nu_s PO_2^- M$ and suggest a potential means of determining the distribution of interacting ions in mixed metal ion environments. The inner-sphere coordination interaction that gives rise to $\nu_s PO_2^- M$ predicts that the strength of the metal−nonbridging phosphate interaction should contribute significantly to the frequency of this vibrational mode. Different degrees of metal-induced shifts of $\nu_s PO_2^-$ to higher wavenumbers for different metal ions have been reported in the literature (*13, 14*); however, no systematic analysis or correlation to absolute electronegativity has been reported previously. As noted above, we observe a linear dependence of the degree of the $\nu_s PO_2^-$ shift to higher wavenumbers ($\Delta\nu M$) on the absolute electronegativity and the absolute hardness of alkali and alkaline earth metals (Figure 6 and Figure S2 of the Supporting Information). Importantly, the differences in $\Delta\nu M$ values for individual metal ions are often in excess of experimental error and could be used to identify or distinguish between individual metal ions. With the exception of that of Li^+, differences in $\Delta\nu M$ are not sufficient to distinguish between individual monovalent ions. However, differences in $\Delta\nu M$ are large enough to distinguish between some divalent ions (e.g., Mg^{2+} and Ca^{2+}) and more generally between mono- and divalent ions. The ability to identify a specific metal ion type is particularly important under conditions where multiple metal ion species are present. Biologically active forms of many structural and catalytic RNAs, for example, involve the binding of both mono- and divalent metal ions, such as Na^+ and Mg^{2+}. We find that $\Delta\nu M$ features for Na^+ and Mg^{2+} are easily resolved in all phosphodiester model systems tested from the simple phosphodiester model system of DMP through the full range of structurally distinct RNAs. The measured values of $\Delta\nu M$ in the model systems mentioned above, nevertheless, represent the average

extents of metal-induced $\nu_s PO_2^-$ shifts of all phosphodiesters in the sample and do not provide information about an individual phosphate position. The Raman signal, however, can provide site-specific information when combined with other biochemical information and parallel Raman analysis of differently modified compounds (*38*).

The concentration of metal ion required to determine $\Delta\nu M$ varies with the metal affinity of the individual phosphodiester compound. High metal ion concentrations ($\sim 1-3$ M) were required to measure $\Delta\nu M$ in DMP, while much lower ion concentrations (e.g., 5 mM Mg^{2+} or 100 mM Na^+) can be used to measure $\Delta\nu M$ in polynucleotides such as the 12-nucleotide GAAA tetraloop (Figure 6, data not shown). This finding indicates that the Raman spectroscopic approach described above can be used to monitor metal–phosphate interactions at or near physical levels of ion concentration.

The data presented here also indicate the need for additional caution in interpretation of metal–phosphodiester interactions from spectroscopic features in addition to $\nu_s PO_2^- M^{PN}$. Attenuation of $\nu_s PO_2^-$, for example, is evident in the Raman spectra of all metal ions we have tested, including transition metals. Our findings, however, indicate that electrostatic and H-bonding interactions can contribute significantly to the attenuation of $\nu_s PO_2^-$ (Figure 2) and may limit quantitative interpretation of inner-sphere metal ion binding using this spectroscopic signal. In addition, we observed, like other studies, that metal ion binding could also be monitored by changes in the Raman spectrum of a nucleotide base (Figure 5B,E). We find, however, that metal-dependent changes in the Raman signal for the adenine base are far more complex than those observed for $\nu_s PO_2 M$. Specifically, they reveal additional influences of structural changes or electrostatic effects beyond saturable ligand binding and should be carefully interpreted even for simple model systems such as ATP or ADP.

In summary, the data presented above enhance the quantitative and interpretive power of Raman analysis of metal–phosphodiester interactions. In particular, these findings help to describe the physical basis for the observed metal-dependent changes in $\nu_s PO_2^-$ that occur in different phosphodiester compounds and in the presence of different metal ions in solution. Such an understanding increases the ability to interpret the extent to which direct and indirect interactions contribute to individual metal ion interactions and, in some cases, to identify or distinguish between individual metal ion species.

It is important to keep in mind that Raman spectroscopic analysis in solution typically requires the ability to obtain samples that are both concentrated (e.g., 20 mg/mL RNA) and highly purified. Practical application of Raman spectroscopy for the quantitative analysis of metal–phosphate interactions in solution is thus currently best suited for the study of relatively small and structurally well-defined model systems such as the ones used in this study. Within this experimental constraint, however, many important questions regarding the nature of metal–phosphate interactions can now be addressed quantitatively. In particular, the Raman spectroscopic method described above provides a potential means of characterizing the distribution of ion binding interactions to RNA and thus information relevant to the ion-dependent folding of RNA and the stabilization of its three-dimensional structure. Quantitative computational studies of ion binding using nonlinear Poisson–Boltzmann theory (*8, 39*) along with direct ion counting methods involving equilibrium dialysis in combination with dye binding fluorescence and atomic emission spectroscopy (*40–42*) have been used to define the counterion atmosphere as a diffuse continuum up to ≥ 10 Å from the nucleic acid surface. Raman spectroscopy provides an opportunity to test and refine these models by measuring the fraction of the counterion atmosphere directly bound to the negatively charged phosphate backbone.

SUPPORTING INFORMATION AVAILABLE

Cobalt hexamine competition for Mg^{2+} binding to ATP, dependence of $\Delta\nu M$ on the absolute hardness of alkali, alkaline earth, and transition metals, examples of raw and difference spectral data of DMP in the presence of different metal ions, and the dependence of $\Delta\nu M$ on metal ion concentration. This material is available free of charge via the Internet at http://pubs.acs.org.

REFERENCES

1. Sigel, R. K., and Pyle, A. M. (2007) Alternative roles for metal ions in enzyme catalysis and the implications for ribozyme chemistry. *Chem. Rev. 107*, 97–113.
2. Stefan, L. R., Zhang, R., Levitan, A. G., Hendrix, D. K., Brenner, S. E., and Holbrook, S. R. (2006) MeRNA: A database of metal ion binding sites in RNA structures. *Nucleic Acids Res. 34*, D131–D134.
3. Lilley, D. M. (2005) Structure, folding and mechanisms of ribozymes. *Curr. Opin. Struct. Biol. 15*, 313–323.
4. Feig, A. L., and Uhlenbeck, O. C. (1999) The Role of Metal Ions in RNA Biochemistry. In The RNA World (Cech, T. R., Gesteland, R. F., and Atkins, J. F., Eds.) pp 287– 320, Cold Spring Harbor Laboratory Press, Plainview, NY.
5. Misra, V. K., Shiman, R., and Draper, D. E. (2003) A thermodynamic framework for the magnesium-dependent folding of RNA. *Biopolymers 69*, 118–136.
6. Misra, V. K., and Draper, D. E. (2002) The linkage between magnesium binding and RNA folding. *J. Mol. Biol. 317*, 507–521.
7. Misra, V. K., and Draper, D. E. (2001) A thermodynamic framework for Mg^{2+} binding to RNA. *Proc. Natl. Acad. Sci. U.S.A. 98*, 12456–12461.
8. Misra, V. K., and Draper, D. E. (2000) Mg^{2+} binding to tRNA revisited: The nonlinear Poisson-Boltzmann model. *J. Mol. Biol. 299*, 813–825.
9. Misra, V. K., and Draper, D. E. (1998) On the role of magnesium ions in RNA stability. *Biopolymers 48*, 113–135.
10. Spiro, T. G. (1987) Biological Applications of Raman Spectroscopy, John Wiley & Sons Inc., New York.
11. Carey, P. R. (1982) Biochemical Applications of Raman and Resonance Raman Spectroscopies, Academic Press Inc., New York.
12. Gong, B., Chen, Y., Christian, E. L., Chen, J. H., Chase, E., Chadalavada, D. M., Yajima, R., Golden, B. L., Bevilacqua, P. C., and Carey, P. R. (2008) Detection of innersphere interactions between magnesium hydrate and the phosphate backbone of the HDV ribozyme using Raman crystallography. *J. Am. Chem. Soc. 130*, 9670–9672.
13. Duguid, J., Bloomfield, V. A., Benevides, J., and Thomas, G. J., Jr. (1993) Raman spectroscopy of DNA-metal complexes. I. Interactions and conformational effects of the divalent cations: Mg, Ca, Sr, Ba, Mn, Co, Ni, Cu, Pd, and Cd. *Biophys. J. 65*, 1916–1928.
14. Stangret, J., and Savoie, R. (1992) Vibrational spectroscopic study of the interaction of metal ions with diethyl phosphate, a model for biological systems. *Can. J. Chem. 70*, 2875–2883.
15. Langlais, M., Tajmir-Riahi, H. A., and Savoie, R. (1990) Raman spectroscopic study of the effects of Ca^{2+}, Mg^{2+}, Zn^{2+}, and Cd^{2+} ions on calf thymus DNA: Binding sites and conformational changes. *Biopolymers 30*, 743–752.
16. Petrov, A. S., Funseth-Smotzer, J., and Paqcl, G. R. (2007) Computational study of dimethyl phosphate anion and its complexes with water, magnesium, and calcium. *Int. J. Quantum Chem. 1–2*, 645–655.

17. Ferre-D'Amare, A. R., Zhou, K., and Doudna, J. A. (1998) Crystal structure of a hepatitis delta virus ribozyme. *Nature 395*, 567–574.

18. Juneau, K., Podell, E., Harrington, D. J., and Cech, T. R. (2001) Structural basis of the enhanced stability of a mutant ribozyme domain and a detailed view of RNA−solvent interactions. *Structure 9*, 221–231.

19. Nakano, S., Proctor, D. J., and Bevilacqua, P. C. (2001) Mechanistic characterization of the HDV genomic ribozyme: Assessing the catalytic and structural contributions of divalent metal ions within a multichannel reaction mechanism. *Biochemistry 40*, 12022–12038.

20. Schmitz, M., and Tinoco, I., Jr. (2000) Solution structure and metal-ion binding of the P4 element from bacterial RNase P RNA. *RNA 6*, 1212–1225.

21. Cowan, J. A. (1993) Metallobiochemistry of RNA. $Co(NH_3)_6^{3+}$ as a probe for Mg^{2+}(aq) binding sites. *J. Inorg. Biochem. 49*, 171–175.

22. Pecoraro, V. L., Hermes, J. D., and Cleland, W. W. (1984) Stability constants of Mg^{2+} and Cd^{2+} complexes of adenine nucleotides and thionucleotides and rate constants for formation and dissociation of MgATP and MgADP. *Biochemistry 23*, 5262–5271.

23. Jaffe, E. K., and Cohn, M. (1979) Diastereomers of the nucleoside phosphorothioates as probes of the structure of the metal nucleotide substrates and of the nucleotide binding site of yeast hexokinase. *J. Biol. Chem. 254*, 10839–10845.

24. Smith, R., and Alberty, R. A. (1956) The Apparent Stability Constants of Ionic Complexes of Various Adenosine Phosphates with Divalent Cations. *J. Am. Chem. Soc. 78*, 2376–2380.

25. Rudisser, S., and Tinoco, I., Jr. (2000) Solution structure of cobalt-(III)hexammine complexed to the GAAA tetraloop, and metal-ion binding to G·A mismatches. *J. Mol. Biol. 295*, 1211–1223.

26. Eckstein, F. (1985) Nucleoside phosphorothioates. *Annu. Rev. Biochem. 54*, 367–402.

27. Steinke, C. A., Reeves, K. K., Powell, J. W., Lee, S. A., Chen, Y. Z., Wyrzykiewicz, T., Griffey, R. H., and Mohan, V. (1997) Vibrational analysis of phosphorothioate DNA: II. The POS group in the model compound dimethyl phosphorothioate [$(CH_3O)_2(POS)$]. *J. Biomol. Struct. Dyn. 14*, 509–516.

28. Sigel, R. K. O., Song, B., and Sigel, H. (1997) Stabilities and Structures of Metal Ion Complexes of Adenosine 5′-O-Thiomonophosphate ($AMPS^{2-}$) in Comparison with Those of Its Parent Nucleotide (AMP^{2-}) in Aqueous Solution. *J. Am. Chem. Soc. 119*, 744–755.

29. Lanir, A., and Yu, N. T. (1979) A Raman spectroscopic study of the interaction of divalent metal ions with adenine moiety of adenosine 5′-triphosphate. *J. Biol. Chem. 254*, 5882–5887.

30. Scheller, K. H., Hofstetter, F., Mitchell, P. R., Prijs, B., and Sigel, H. (1981) Macrochelate formation in monomeric metal ion complexes of nucleoside 5′-triphosphates and the promotion of stacking by metal ions. Comparison of the self-association of purine and pyrimidine 5′-triphosphates using proton nuclear magnetic resonance. *J. Am. Chem. Soc. 103*, 247–260.

31. Reily, M. D., Hambley, T. W., and Marzilli, L. G. (1988) Macrochelate complexes of purine 5′-nucleotide triphosphates and monophosphates: Definitive multinuclear NMR evidence supported by molecular mechanics calculations. *J. Am. Chem. Soc. 110*, 2999–3007.

32. Bianchi, E. M., Sajadi, S. A., Song, B., and Sigel, H. (2003) Stabilities and isomeric equilibria in aqueous solution of monomeric metal ion complexes of adenosine 5′-diphosphate (ADP^{3-}) in comparison with those of adenosine 5′-monophosphate (AMP^{2-}). *Chemistry 9*, 881–892.

33. Takeuchi, H., Murata, H., and Harada, I. (1988) Interaction of adenosine 5′-triphosphate with Mg^{2+}: Vibrational study of coordination sites by use of ^{18}O-labeled triphosphates. *J. Am. Chem. Soc. 110*, 392–397.

34. Pearson, R. G. (1988) Absolute Electronegativity and Hardness: Application to Inorganic Chemistry. *Inorg. Chem. 27*, 734–740.

35. Shelton, V. M., Sosnick, T. R., and Pan, T. (2001) Altering the intermediate in the equilibrium folding of unmodified yeast tRNAPhe with monovalent and divalent cations. *Biochemistry 40*, 3629–3638.

36. Shelton, V. M., Sosnick, T. R., and Pan, T. (1999) Applicability of urea in the thermodynamic analysis of secondary and tertiary RNA folding. *Biochemistry 38*, 16831–16839.

37. Shi, H., and Moore, P. B. (2000) The crystal structure of yeast phenylalanine tRNA at 1.93 Å resolution: A classic structure revisited. *RNA 6*, 1091–1105.

38. Chen, J. H., Gong, B., Bevilacqua, P. C., Carey, P. R., and Golden, B. L. (2009) A catalytic metal ion interacts with the cleavage site G·U wobble in the HDV ribozyme. *Biochemistry 48*, 1498–1507.

39. Sharp, K. A., and Honig, B. (1995) Salt effects on nucleic acids. *Curr. Opin. Struct. Biol. 5*, 323–328.

40. Bai, Y., Greenfeld, M., Travers, K. J., Chu, V. B., Lipfert, J., Doniach, S., and Herschlag, D. (2007) Quantitative and comprehensive decomposition of the ion atmosphere around nucleic acids. *J. Am. Chem. Soc. 129*, 14981–14988.

41. Das, R., Travers, K. J., Bai, Y., and Herschlag, D. (2005) Determining the Mg^{2+} stoichiometry for folding an RNA metal ion core. *J. Am. Chem. Soc. 127*, 8272–8273.

42. Grilley, D., Soto, A. M., and Draper, D. E. (2006) Mg^{2+}-RNA interaction free energies and their relationship to the folding of RNA tertiary structures. *Proc. Natl. Acad. Sci. U.S.A. 103*, 14003–14008.

43. Guan, Y., Wurrey, C. J., and Thomas, G. J. (1994) Vibrational analysis of nucleic acids. I. The phosphodiester group in dimethyl phosphate model compounds: $(CH_3O)_2PO_2^-$, $(CD_3O)_2PO_2^-$, and $(^{13}CH_3O)_2PO_2$. *Biophys. J. 66*, 225–235.